A Four-State Scheme for Treating Polymer Crystallization and Melting Suggested by Calorimetric and Small Angle X-ray Scattering Experiments on Syndiotactic Polypropylene†

ARTICLE *in* MACROMOLECULES · SEPTEMBER 1997

Impact Factor: 5.8 · DOI: 10.1021/ma9703923

3 AUTHORS, INCLUDING:

Juergen Schmidtke
Universität Paderborn
21 PUBLICATIONS **800** CITATIONS

SEE PROFILE

A Four-State Scheme for Treating Polymer Crystallization and Melting Suggested by Calorimetric and Small Angle X-ray Scattering Experiments on Syndiotactic Polypropylene†

J. Schmidtke,‡ G. Strobl,*,‡ and T. Thurn-Albrecht§

Fakultät für Physik der Albert-Ludwigs-Universität, 79104 Freiburg, Germany, and Max-Planck-Institut für Polymerforschung, 55021 Mainz, Germany

Received March 20, 1997⊗

ABSTRACT: As shown by time- and temperature dependent SAXS experiments, crystals of s-PP do not change their thickness during isothermal crystallization and a subsequent heating to melting. This allows an accurate determination of the relations between crystallization temperature, crystallite thickness, rate of crystallization, and melting points. There are five main results obtained in a comprehensive SAXS and DSC investigation: (i) Crystals have greatly varying stabilities, in spite of their uniform thickness; the first crystals melt close to the crystallization temperature. (ii) Melting points are affected by the distance to neighboring crystals. (iii) Crystals perfect during heating and annealing. (iv) Recrystallization after melting, as observed for low enough heating rates, starts with crystal growth rates that are at least 2 orders of magnitude higher than for a primary crystallization, and then slows down progressively, being accompanied by an increase in crystal thickness. (v) The dynamic signals observed in a MDSC run are indicative of a smooth change between crystallization and melting at the growth front. Data evaluation yields the average time required for a melting of individual crystallites. A *four-state* scheme allows a description of the behavior. It is based on the following assumptions: (i) Primary crystallization from the *melt* produces in a first step imperfect "*native*" *crystals*, which are subsequently stabilized by structural relaxation processes. These affect both the interior and the surface region. Crystallization proceeds under a small driving force, near to the equilibrium between melt and native crystals. (ii) The amount of structural relaxation is nonuniform thus producing crystals of different stability. (iii) With increasing crystallization temperature, i.e., decreasing growth rate, native crystals continuously approach the equilibrium state. (iv) The main part of fusion takes place near the equilibrium between the *relaxed crystals* and the *disentangled melt*.

1. Introduction

The development of new metallocene catalysts which can produce nearly perfect syndiotactic polypropylene[1] has renewed the interest in these polymers and initiated a number of detailed studies of their morphology, crystalline structure, and thermal properties. Syndiotactic polypropylene (s-PP) is partially crystalline. If the crystallization is carried out in thin films,[2,3] the crystallites can be observed directly by electron microscopy and atomic force microscopy (AFM). One finds large single crystals with a rectangular, lath-shaped habit. The two edges differ in character. While the long edge is straight, indicating a microscopically planar lateral surface, the short edge always shows some curvature indicative for a roughened structure. If the crystallization is conducted at elevated temperatures, above 120 °C, bundles of crystallites form that emanate from a common nucleus. At lower temperatures, the crystallites become organized in spherulites, dendrites or axialites, indicative of a stronger splaying and branching during crystal growth.

We now have also a good knowledge of the crystal structure. As known since the early work of Nata and Corradini,[4] the chain conformation corresponds to a g_2t_2 sequence for each syndiotactic repeat unit, setting up a helix of two syndiotactic units per turn with a period of 0.74 nm. The mode of chain packing in the crystals has been established only recently, in electron diffraction studies on single crystals by Lovinger and Lotz.[5] Figure 1 depicts this crystal structure (addressed in the literature as "type III"). The unit cell is orthorhombic and occupied by two left- and two right-handed helices. The interaction energy between the chains is highly anisotropic. There is a strong coupling along the *b*-axis. On the other hand, the rows of chains along *b* may easily be displaced against each other, by relative shifts of $b/4$ or $b/2$, thus creating a characteristic disorder. The disorder becomes reduced when increasing the temperature, and for temperatures above 130 °C crystallites appear to be well-ordered. It is due to the strong intermolecular interaction that the long edge, along *b*, is microscopically smooth. Under this condition, it became even possible to observe directly the pairing of right- and left-handed helices along the row in the atomic force microscope.[5] On the other hand, the roughening of the short edge, along *a*, may originate from the frequent occurrence of the glide processes. The observed growth rates agree with these conditions. They are large in *b*-direction, i.e., for the *ac* growth face. This face always contains many niches, which are necessary for encorporating new crystalline stems. On the other hand, growth rates are much smaller along *a*, because here we have a smooth growth face that includes only a very low number of niches, if at all. As an important further observation, atomic force microscopy indicates that the single crystals are covered by 6 nm thick disordered layers with a structureless surface. As proved by microdrawing experiments, chain connections through the surface layer have no preferred orientation, going equally along the *a*- and the *b*-axes.[6]

Studies of crystallization and melting were carried out as a function of the content of racemic units and the molecular weight, mainly by differential scanning cal-

* To whom correspondence should be addressed.
† Dedicated to Professor E. W. Fischer.
‡ Albert-Ludwigs-Universität.
§ Max-Planck-Institüt für Polymerforschung.
⊗ Abstract published in *Advance ACS Abstracts,* September 1, 1997.

S0024-9297(97)00392-6 CCC: $14.00

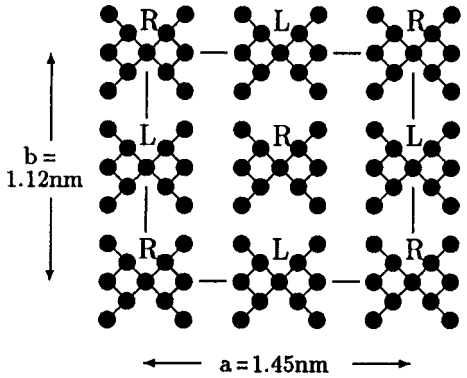

Figure 1. Unit cell of s-PP in a view along the chain axes. The cell is orthohombic and passed by two right-and two left-handed helices.

orimetry. One observes a systematic shift of the temperatures of crystallization and melting to lower values with increasing content of meso units.[7] Molecular weight effects essentially vanish for molecular masses above 40 000 g/mol.[3] Measured crystallization isotherms can be represented by the Avrami function. The derived characteristic time of crystallization shows the usual exponential decreases with increasing temperature. The heats of fusion given in the literature vary somewhat, between 6.9[7] and 8.4 kJ mol^{-1} [8] (referring to propylene units C_3 H_6).

In polyethylene, at elevated temperatures chains possess a longitudinal mobility in the crystalline state that is provided by the α-process. As a consequence, surface crystallization and melting as well as crystal-thickening processes within the solid state become possible.[9,10] Furthermore, the cold-drawing behavior is affected, because the internal mobility improves the drawability. An α-process with similar properties is also found in isotactic polypropylene, but not in s-PP.[11] This fact makes syndiotactic polypropylene a good candidate for fundamental studies of the mechanism of crystallization. In polyethylene, we have the complications arising from the ongoing crystal thickening and the surface crystallization and melting; in isotactic polypropylene usually cross-hatching processes lead to a complex structure. In s-PP we find neither of these features and encounter a favorable situation, having a well-defined morphology with stacks of laterally extended lath-shaped crystallites, at least in the high-temperature range (>120 °C). We therefore chose this system for a detailed study of the structure changes during crystallization and melting, employing temperature- and time-dependent small-angle X-ray scattering experiments. It was possible to determine simultaneously all parameters necessary for a thorough analysis of the crystallization kinetics, namely for a given crystallization temperature T_c, the crystal thickness d_c, the growth rate u, and in addition, by carrying out a heating experiment subsequent to the primary crystallization, the limit of stability of the formed crystals. We complemented the scattering experiments by specific calorimetric studies including a modulated DSC run and finally arrived at a set of data that, to our knowledge, is more accurate and complete than for any other polymer.

Absence of reorganization processes in the solid state as promoted by the α-process does not mean that there is no restructuring at all. There were reports in the literature that clearly indicated a change of structure by a recrystallization immediately after melting,[3,12] We studied this melting−recrystallization process in more detail, in particular to compare its rate with the rates of primary crystallization at the same temperature. Furthermore, we determined the thicknesses of the newly formed crystallites.

After completion of the primary crystallization at T_c, a subsequent cooling to room temperature always leads to a further "secondary" crystallization. We analyzed the associated structural changes by SAXS experiments. As it turned out, secondary crystallization occurs by the "insertion mode", (Chapter 4.3 in ref 13), and we determined the thicknesses and stability limits of the inserted crystallites.

The motivation of our studies was the search for a complete set of data that would enable us to check and reconsider the current views on polymer crystallization and melting. Indeed, the experiments led us to several definite conclusions about some basic properties and suggested the introduction of a "four-state model" as an appropriate scheme for treating these phenomena. It will be explained after the discussion, in the final section of this paper.

2. Experimental Section

2.1. Sample. The syndiotactic polypropylene used in the experiments was synthesized by S. Jüngling in the group of Prof. Mülhaupt in the Institute of Macromolecular Chemistry of our university. The product had 91% racemic pentads (97% racemic triads), as determined by ^{13}C NMR. The number average molecular weight as obtained by GPC was M_n=1.04 × 10^5 (M_w/M_n = 2.3). More details about the sample and morphological observations are reported in ref 14. In particular, AFM studies on etched films provided insight into the structure. For a crystallization temperature of 135 °C, one finds bundles of lath-shaped lamellar crystallites with a thickness of about 10 nm.

2.2. Instrumentation. Conventional DSC curves were registered with the aid of a Perkin-Elmer calorimeter model DSC 4. In addition, Dr. Schawe (IFA Ulm) provided us with an MDSC measurement carried out with a Perkin-Elmer DSC 7.

SAXS experiments were conducted using a conventional X-ray tube and a Kratky camera equipped with a temperature-controlled sample holder. Intensities were measured by both a scintillation counter together with a step scanning device and, in time-dependent investigations, a position-sensitive metal wire detector. In the latter case, values of sufficient accuracy were obtained within a few minutes counting time. As the camera is equipped with a slit focus, data had to be deconvoluted. This was achieved by applying a desmearing algorithm developed in our group.[15]

2.3. MDSC Data Representation. Generally, in differential scanning calorimetry the heat flux dQ/dt into the sample is monitored during a programmed temperature change. In an MDSC run the time-dependent temperature is given by

$$T(t) = T(0) + \beta t + \Delta T_0 \sin \omega t \qquad (1)$$

implying a superposition of a linear increase of temperature with a rate β and an oscillatory part with amplitude ΔT_0 and frequency ω.[16] In the absence of the oscillatory part, i.e., in the case of a conventional DSC run, we write

$$\frac{dQ}{dt} = c_1 \frac{dT}{dt} = c_1 \beta \qquad (2)$$

with c_l denoting the normal "underlying" heat capacity. c_l is understood as including both the specific heats of all parts in the sample and also all enthalpy changes following from phase transitions. The modulated part is associated with a reversible heat exchange between the sample and the heating device. In the general case, a phase lag may arise between the temper-

ature change dT/dt and the heat flux. In order to account for this possible effect, one writes

$$\frac{dQ}{dt} = c_1\beta + c_v\Delta T_0\omega\cos(\omega t - \alpha) = c_1\beta + c_v'\Delta T_0\omega\cos\omega t + c_v''\Delta T_0\omega\sin\omega t \quad (3)$$

Here, c_v and α denote the amplitude and phase lag associated with this "dynamic" heat capacity. An equivalent description uses the real and imaginary part of c_v, denoted c_v' and c_v''. The real part is associated with that part of the heat flux that is in phase with the time derivative of the temperature, i.e. the instantaneous heating rate; the imaginary part has a phase lag of $\pi/2$. In this work, data will be given in terms of c_l, c_v' and c_v''.

2.4. SAXS Data Analysis. For the system under study, being made of stacks of thin laterally extended crystallites, the scattering intensity can be related to the one-dimensional electron density correlation function $K(z)$ defined as

$$K(z) = \langle(\rho_e(z) - \langle\rho_e\rangle)(\rho_e(0) - \langle\rho_e\rangle)\rangle = \langle\rho_e(z)\rho_e(0)\rangle - \langle\rho_e\rangle^2 \quad (4)$$

It can be directly obtained by a Fourier transformation of the scattering intensity. If we use the scattering cross-section per unit volume, $\Sigma(q)$, $K(z)$ follows as

$$K(z) = \frac{1}{r_e^2}\frac{1}{(2\pi)^3}\int_0^\infty \cos qz\, 4\pi q^2\Sigma(q)\, dq \quad (5)$$

q denotes the modulus of the scattering vector, being related to the Bragg scattering angle, ϑ_B, by

$$q = \frac{4\pi}{\lambda}\sin\vartheta_B \quad (6)$$

The parameter r_e is the classical electron radius, $r_e = 2.81 \times 10^{-15}$ m.

In the case of partially crystallined polymers, a trajectory along the surface normal passes through amorphous regions with an electron density $\rho_{e,a}$ and crystallites with a core density $\rho_{e,c}$. As shown by Ruland,[17] for such a layer system the second derivative of the correlation function, $K''(z)$, gives the distribution of distances between interfaces, in the form

$$K''(z) = \frac{O_{ac}}{2}\Delta\rho_e^2[h_a(z) + h_c(z) - 2h_{ac}(z) + h_{aca}(z) + h_{cac}(z)...] \quad (7)$$

The expression between the brackets is made of a series of distribution functions, whereby the subscripts indicate which phases, amorphous and crystalline ones, are to be traversed while going from one interface to the other. Of main importance are the first three contributions. They give the distributions of the thickness of the amorphous and the crystalline layers, respectively (h_a, h_c) and of the sum of both (h_{ac}), which is identical with the long spacing L. If the boundaries between the crystalline and the amorphous regions are sharp within the resolution limit of SAXS experiments, the asymptotic behavior of $\Sigma(q)$ in the limit of large scattering angles is given by Porod's law

$$\lim_{q\to\infty}\Sigma(q) = r_e^2\frac{P}{(q/2\pi)^4} \quad (8)$$

Hereby P denotes the Porod parameter which is directly related to the specific internal surface O_{ac}, i.e., the area per unit volume of the interface separating crystalline and amorphous regions, by

$$P = \frac{1}{8\pi^3}O_{ac}\Delta\rho_e^2 \quad (9)$$

Rather than by taking the second derivative of the correlation function, $K''(z)$ can also be deduced directly from the measuring data, by use of

$$K''(z) = \frac{2}{r_e^2(2\pi)^2}\int_0^\infty[\lim_{q\to\infty} q^4\Sigma(q) - q^4\Sigma(q)]\cos qz\, dq \quad (10)$$

The correlation function $K(z)$ has a characteristic shape (Chapter A.4.2 in ref 13). It is composed of a sequence of contributions that reflect the correlations within one crystallite, between next neighbors, second neighbors, etc. The most important part is the "self-correlation triangle" centered at the origin. It exhibits several characteristic properties. If the sample is homogeneously filled with stacks of crystallites, the value at $z = 0$, known as the "invariant", can be directly related to the volume fraction of the crystallites ϕ_c, by

$$K(z=0) = \phi_c(1-\phi_c)\Delta\rho_e^2 \quad (11)$$

It can be shown that the slope dK/dz is directly related to the Porod parameter and yields also O_{ac}, by

$$\frac{dK}{dz} = -\frac{O_{ac}}{2}\Delta\rho_e^2 \quad (12)$$

A further parameter, l_c, is obtained by taking the ratio between the invariant, $K(0)$, and the initial slope, $K'(0)$

$$\frac{K(0)}{K'(0)} = l_c = \frac{2\phi_c(1-\phi_c)}{O_{ac}} \quad (13)$$

l_c characterizes the length scale of the two-phase structure. Knowing the crystallinity ϕ_c and the specific internal surface, one may derive the crystallite thickness, d_c, by use of the general relation

$$\phi_c = \frac{O_{ac}}{2}d_c \quad (14)$$

From the two last equations there follows

$$l_c = d_c\left(1 - \frac{O_{ac}}{2}d_c\right) \quad (15)$$

or reversely

$$d_c = \frac{1}{O_{ac}} - \left(\frac{1}{O_{ac}^2} - \frac{2l_c}{O_{ac}}\right)^{1/2} \quad (16)$$

As an approximation, the specific internal surface may be related to the long-spacing L, by

$$O_{ac} \approx \frac{2}{L} \quad (17)$$

The relation can be used together with eq 16 to obtain the crystallite thickness, if l_c and L (but not O_{ac}) are known. Equation 17 may also be employed for an approximate determination of the electron density difference between the amorphous and crystalline regions, $\Delta\rho_e$. We write

$$\Delta\rho_e^2 = \frac{K'(0)}{O_{ac}/2} \approx LK'(0) \quad (18)$$

Evaluation of the experimental data led us to the following linear temperature dependence of $\Delta\rho_e$

$$\Delta\rho_e(T/°C) = (29.9 + 0.105T)\ \text{nm}^{-3} \quad (19)$$

3. Results

3.1. Isothermal Crystallization and Subsequent Melting. After samples were kept in the melt at 190 °C for 30 min, they were cooled in the Kratky camera

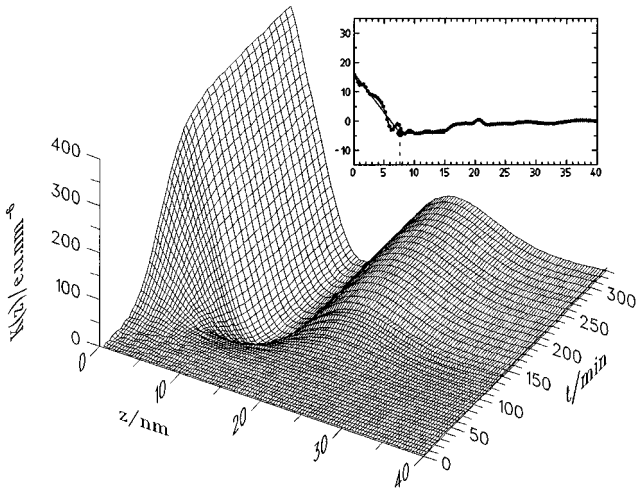

Figure 2. Isothermal crystallization of s-PP at $T_c = 133$ °C followed by time-dependent SAXS. Derived electron-density correlation functions. The inset shows the correlation function measured after 52.5 min, indicative of crystals with a thickness of 7.5 nm.

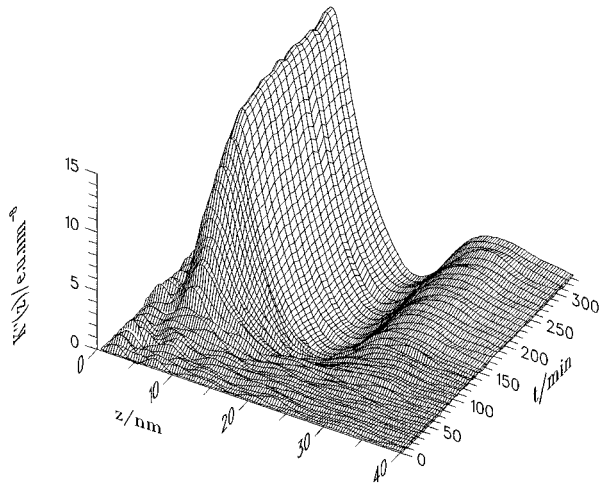

Figure 3. Same experiment as Figure 2: Function $K''(z)$ giving the distribution function of interface distances.

as fast as possible to the crystallization temperature, chosen in the range between 122 and 140 °C. By observation of the intensity, it was made sure that crystallization did not start before isothermal conditions were achieved. Then, the development of the structure was followed by time-dependent small angle X-ray scattering experiments. Figure 2 shows as an example the result of an experiment carried out at the crystallization temperature $T_c = 133$ °C. The three-dimensional plot presents the one-dimensional electron density correlation function, $K(z)$, as it evolves as a function of time. In the initial stage, for times below 50 min, $K(z)$ is given by the "self-correlation triangle" only, as is indicative for the occurrence of individual crystallites. The inset depicts one of these curves. As indicated by the width of the base of the triangle, the crystallite thickness amounts to $d_c = 7.5$ nm. Then, when time goes on, a stack is formed. The peak around 23 nm gives the long spacing of the final structure. Equivalent information can be derived from the second derivative, $K''(z)$. According to eq 7, $K''(z)$ relates to the distribution of distances between the interfaces in the stack. Figure 3 shows the functions $K''(z)$ derived from the same scattering curves as in the case of Figure 2, i.e., during an isothermal crystallization at 133 °C. We observe a dominant ridge located with its maximum

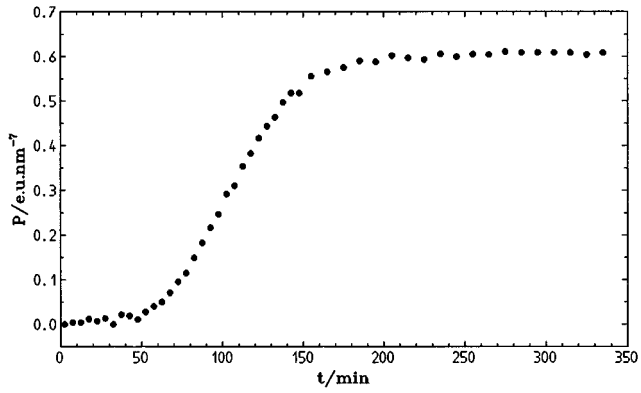

Figure 4. Same experiment as Figure 2: Time dependence of the Porod parameter.

at 7.5 nm. Obviously, it again reflects the crystallites and their thickness. Interestingly, the ridge location remains constant throughout the whole crystallization process. In $K''(z)$, the long spacing shows up as a minimum, located at 23 nm. In striking contrast to the crystallites with their uniform thickness, the thicknesses of the amorphous layer in between are broadly distributed. The average value should lie around 23−7.5 nm ≈ 15 nm, but it is not associated with a peak.

The kinetics of crystallization may be conveniently expressed by use of the Porod parameter, P. According to eq 9, P is always proportional to the specific internal surface. This relation holds through all times, from the initial stage with its heterogeneous sample structure up to the end, when the sample is completely filled with stacks of crystallites. Since the crystallite thickness does not change with time, the degree of crystallization follows the same curve. Figure 4 depicts the time dependence of the Porod parameter as obtained for the experiment of Figures 2 and 3. As usual for polymers we observe a curve with sigmoidal shape, which indicates in this case a half-time of crystallization on the order of 100 min. After completion of primary crystallization we end up with a value $P = 0.6$ nm^{-7}, corresponding to a specific internal surface $O_{ac} = 7.75 \times 10^{-2}$ nm^{-1}. Regarding that the crystals have a thickness of 7.5 nm, we obtain for the crystallinity with eq 14 $\phi_c = 0.29$. If we estimate ϕ_c by just taking the ratio d_c/L we arrive at a similar result. Direct observations of stacks of crystallites in the EM or AFM may sometimes suggest a higher crystallinity. However, this seems to be a wrong impression. The amorphous regions close to the crystallite surface have a lowered mobility, which may greatly reduce the penetration of the staining or etching agent.

Analoguous experiments were carried out at the other crystallization temperatures. Figure 5 presents in normalized form the kinetic curves, $P(t)/P(\infty)$. As expected, growth rates greatly change with temperature. Curves retain their sigmoidal shape, and it is possible to represent them by use of the Avrami expression

$$P(t) \sim O_{ac} \sim 1 - \exp\left[-\left(\frac{t}{\tau}\right)^{\beta}\right] \qquad (20)$$

The exponent β is essentially constant, with values in the range $\beta = 3.5 \pm 0.2$. Figure 6 shows the characteristic time τ as derived from the Avrami plots at different T_c's. As is common for polymers, a temperature increase results in a near to linear increase of $\log \tau$.

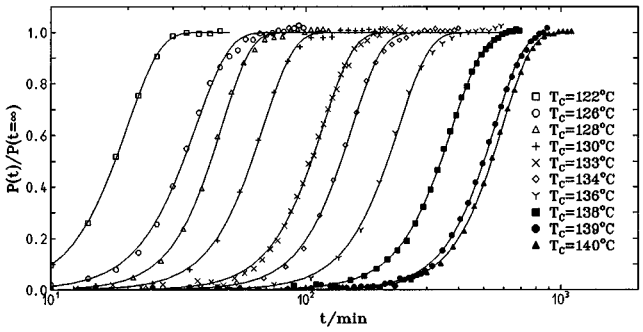

Figure 5. Isothermal crystallization of s-PP conducted at a series of temperatures between 122 and 140 °C, followed by time-dependent measurements of the Porod parameter.

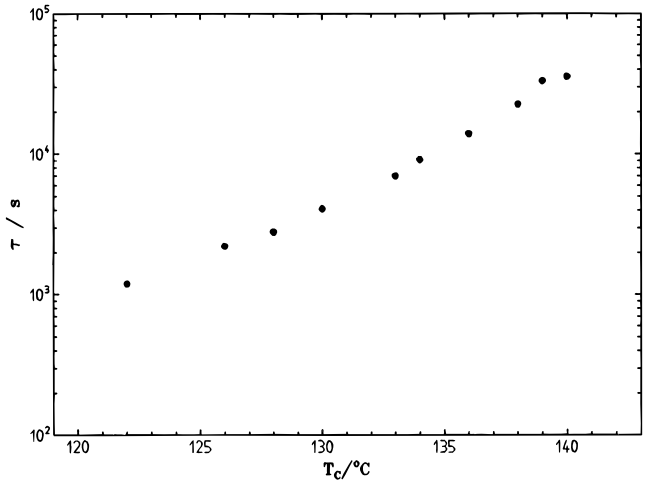

Figure 6. Characteristic times derived from Avrami representations of the isotherms in Figure 5.

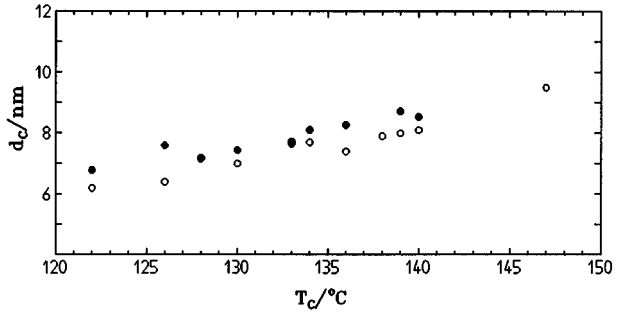

Figure 7. Dependence of the crystallite thickness on the crystallization temperature, derived from $K(z)$ in the initial stage (open symbols) and from global parameters of the completed structure (filled symbols).

The results presented in Figures 2 and 3 are typical ones. For all crystallization temperatures it was found that the crystallite thickness did not change during the process of crystallization. The most accurate measurements of d_c were those in the initial stages, in the absence of intercrystallite interferences. Figure 7 collects all data thus obtained. For a check we derived d_c also from the scattering curve at the end of primary crystallization, employing eq 16 and the approximate relation eq 17. These results are also given in the figure and we find the same tendency with only a small difference in values. As we see, d_c varies between 6 nm at T_c = 122 °C and 9.5 nm at T_c = 147 °C. For the highest temperature, due to the ultralow crystallization rate, measurements were restricted to the initial stage only. Figure 8 shows the correlation functions obtained, which have a perfect triangular shape.

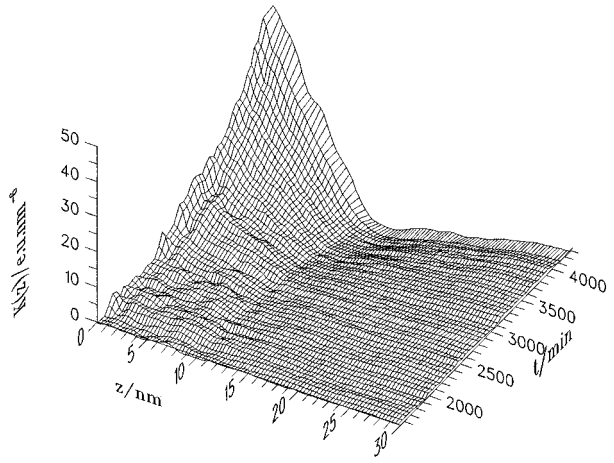

Figure 8. Single crystallite correlation functions obtained for T_c = 147 °C.

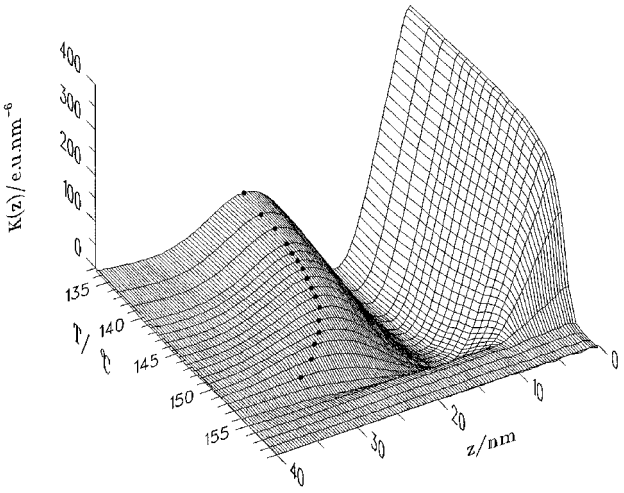

Figure 9. Continuation of the experiment of Figure 2: Observation of the melting during a heating subsequent to the isothermal crystallization. Points indicate the long spacing maxima.

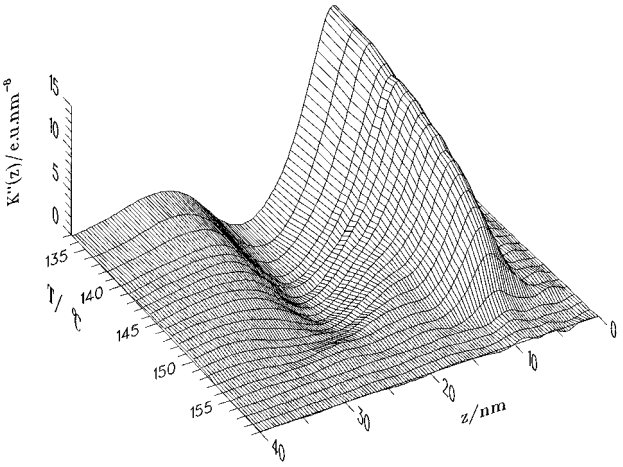

Figure 10. Continuation of the experiment of Figure 3: Observation of the melting during a heating subsequent to the isothermal crystallization.

Next we investigated the stability of the primary crystals by a slow heating subsequent to the completion of primary crystallization. The results obtained for the sample of Figures 2−4 are shown in Figures 9−11. In all the curves, one observes a continuous decrease of the respective values with incrasing temperature. SAXS curves were registered at each of the indicated temper-

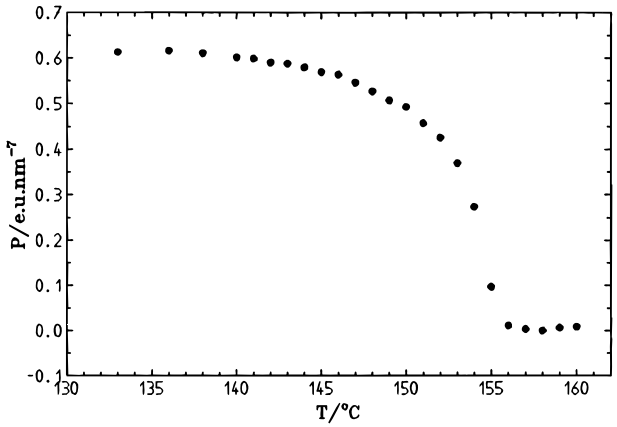

Figure 11. Same experiment as Figure 10: Melting shown by the decrease of the Porod parameter.

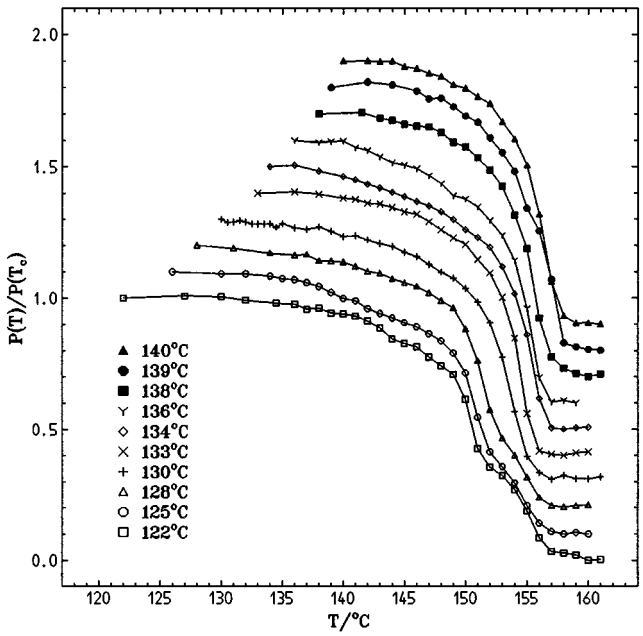

Figure 12. Melting after an isothermal crystallization at the indicated temperatures, registered by measurements of the Porod parameter. Curves are vertically displaced against each other by constant amounts.

atures with a measuring time of 10 min, thus creating a rather low overall heating rate. We note that the ridge position stays absolutely constant, telling us that we have no crystal-thickening processes. Interestingly, crystals, in spite of having a constant thickness, vary in their stability. Melting obviously starts shortly above the crystallization temperature and then increases in rate; the last crystals disappear at 155 °C. Note that the melting rates between T_c and 155 °C are even stronger than indicated by the Porod parameter. P includes as an additional factor the electron density difference $\Delta\rho_e^2$, which increases with temperature, thus acting in reverse direction.

An analogous behavior was found for all crystallization temperatures. Figure 12 collects all melting curves, expressed by the temperature dependence of the Porod parameter in normalized form, $P(T)/P(T_0)$. Obviously, an increase in the crystallization temperature results in an increase of the crystal stability. The temperature with the highest melting rate, T_f, is usually addressed as the "temperature of fusion" of the crystallites. However, we should be aware that even for crystals with a constant thickness, we find no unique melting temperature.

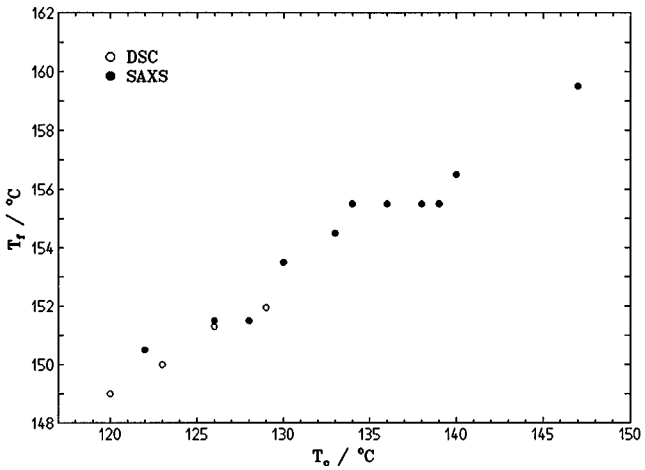

Figure 13. Temperature with the highest melting rate T_f as a function of the crystallization temperature T_c.

A peculiarity arises for the lower T_c's. As indicated in the figure, melting here takes place in two successive steps. As will be discussed later on, this phenomenon is due to a melting immediately followed by recrystallization. Therefore, in the description of the relation between T_f and T_c we have to select the location of the first maximum slope. Figure 13 depicts this dependence, collecting all values of T_f. We compared the results with literature data obtained by DSC for samples with a similar content of racemic units[7] and find a good agreement.

To complement and check the SAXS results, we carried out analogous experiments in a differential calorimeter, by first conducting the isothermal crystallization up to completion and then following the melting during a reheating. Figure 14 depicts melting curves measured after various times of crystallization at 120 °C. The curves have the usual form and are shown here only to stress one important point: In agreement with the SAXS observation, we find again that melting starts immediately above the crystallization temperature, slowly at first and then with increasing rate, reaching the maximum just before the end. The curves further demonstrate that this is true irrespective of the time of crystallization. Figure 13 includes in addition to the SAXS results the values of T_f obtained by differential calorimetry. As we see, DSC and SAXS results confirm each other.

We also determined the heat released during an isothermal crystallization at 130 °C. It amounted to $\Delta H = 53$ J g^{-1}. Combining this value with the crystallinity derived from the SAXS curve, we obtain for the heat of fusion of the s-PP crystallites

$$\Delta H_f = 53 \text{ J g}^{-1}/0.29 = 183 \text{ J g}^{-1} = 7.7 \text{ kJ mol}^{-1}$$

which essentially agrees with the literature data cited in the Introduction. As a remark, we found that the heat of fusion during a subsequent melting was always larger by 5−10%. This difference may reflect the temperature dependence of the heat of fusion, following from the different values of the heat capacities of the crystallites and the amorphous regions.

Employing a modulated differential scanning calorimeter, the curves shown in Figure 15 were obtained. As in the other experiments, observations refer to the melting subsequent to an isothermal crystallization, here conducted at 130 °C. The parameter set of the run is given in the figure caption. The mean heat capacity,

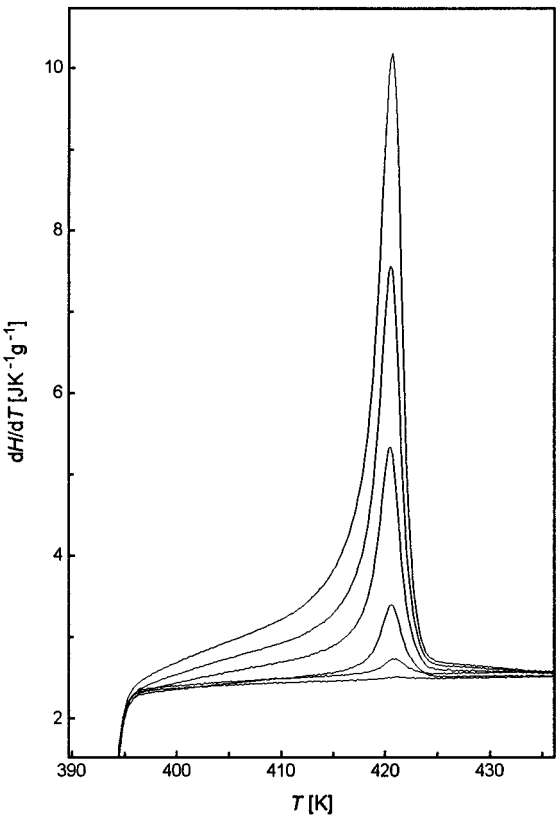

Figure 14. DSC melting curves measured after various periods (2, 4, 6, 8, 10, and 12 min) of isothermal crystallization at $T_c = 120$ °C.

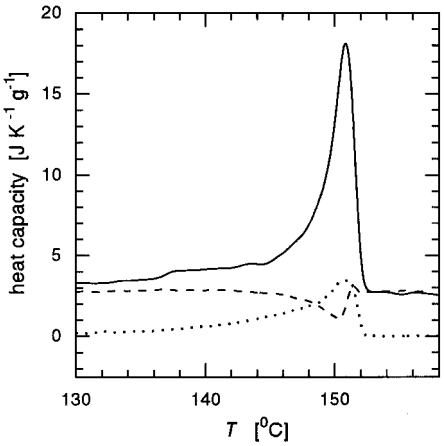

Figure 15. Results of an MDSC run after an isothermal crystallization at $T_c = 130$ °C ($\beta = 0.5$ K min^{-1}, $\omega = 2\pi/96$ s, $\Delta T_0 = 0.2$ K): mean heat capacity c_l (continuous line); real and imaginary part of the dynamic heat capacity, c_v' (dashes) and c_v'' (dots). Measurement by J. Schawe (IFA, Ulm).

c_l, agrees with the result of a conventional DSC run. The interesting point is the existence of the dynamic signals c_v' and c_v''. They demonstrate that rates of melting vary linearly with the temperature. Importantly, as will be explained later on, their occurrence is indicative of reversible changes between melting and crystallization to take place at the growth face of a crystallite. As will also be shown, data evaluation allows an estimate of the times required by the individual crystallites for their melting.

3.2. Crystal Perfectioning and Melting−Recrystallization Processes. There are reports in the literature about the occurrence of double endotherms in the DSC curves indicative for a melting immediately followed by recrystallization.[12] We have carried out a more detailed investigation of this process. As a first result, Figure 16 depicts a series of DSC curves measured directly after the completion of primary crystallization at three different temperatures, employing three different heating rates as specified in the figure. One observes a splitting of the melting peaks coming up for low heating rates. As we see, the weight of the high temperature component increases with decreasing heating rate and with decreasing crystallization temperature T_c. There are also changes in the location of the low-temperature part. Generally, it shifts to higher temperatures with decreasing heating rate; however, for the highest heating rate, a reverse shift is observed. As one can exclude heat conduction effects at a heating rate of 10 K/min, the latter behavior indicates a superheating of the crystallites. Quite remarkable is the sharpening of the first melting peak with decreasing rate. As proposed in ref 12, the new peak coming up on the high-temperature side should be due to a second melting after a recrystallization in the temperature range of the first endotherm.

To check and ensure this assignment, we carried out an additional experiment with the results being shown in Figure 17. A sample was completely crystallized at $T_c = 120$ °C and then heated rapidly to 146 °C, which is right in the center of the main melting region. There, it was kept for different times of annealing before continuing the heating, now with a moderate heating rate of 10 K/min. In the figure we see at first part of the curve that is measured up to the temperature of 146 °C and then, on the right, the curves obtained during the heating after the various annealing times. These final melting curves are composed of two parts. There is a first part that obviously has to be associated with the final melting of the not yet melted material. On the other hand, the second part shows the melting of the already once melted and then recrystallized part of the sample. We separated both contributions by numerical means. The procedure is indicated in Figure 18. For the first part we chose a symmetric Gaussian with a constant integral weight. The second part was described by an asymmetric function made of two half-Gaussians with different widths. It shows a varying overall width and weight, both increasing with annealing time. Figure 19 gives us as the result of the data evaluation the heat contents included in the two parts, as a function of the annealing time. We observe a steady increase of the second part, with the largest rate of increase at the beginning. In quantitative terms, we obtained the following data. The total heat of fusion measured without the interruption step is $\Delta H = 55$ kJ/g. The largest part, namely 50 kJ/g, is already molten at 146 °C. The remaining part is the first component found in the heating after the annealing, with a heat of 5 kJ/g. For the longest times of annealing, we find a heat of fusion of the recrystallized material of about 30 kJ/g, corresponding to about 60% of the molten material. We also have evidence for crystal perfectioning processes. These show up in the shift of the first part to higher temperatures, i.e., higher stabilities.

The occurrence of crystal-perfectioning processes is also indicated by another experiment. As was pointed out by Lovinger and Lotz,[18] the perfectness of the crystal structure may be checked by measuring the intensity of a peculiar reflection characteristic for the "type III" lattice. This 211 reflection is located at a scattering angle $2\vartheta_B = 18.7°$ and can be seen in the series of

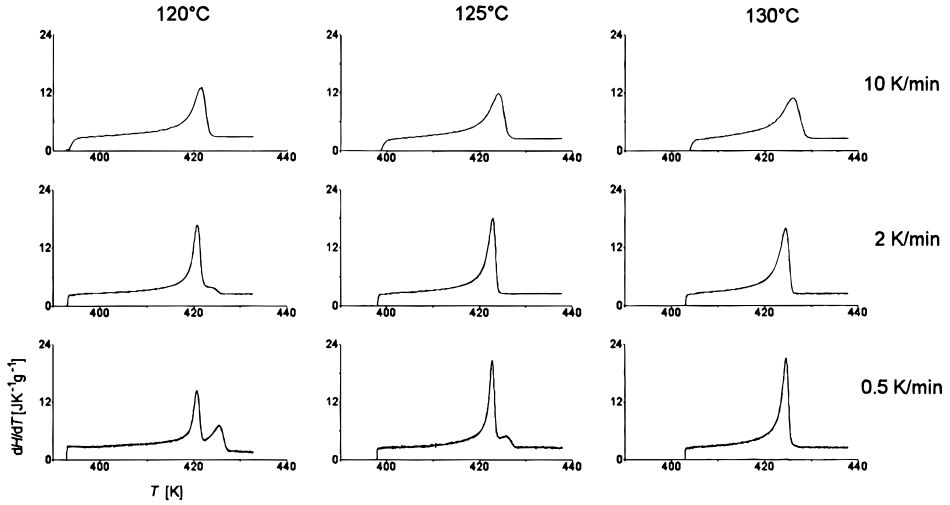

Figure 16. Melting subsequent to isothermal crystallization: DSC curves obtained for different T_c's and heating rates.

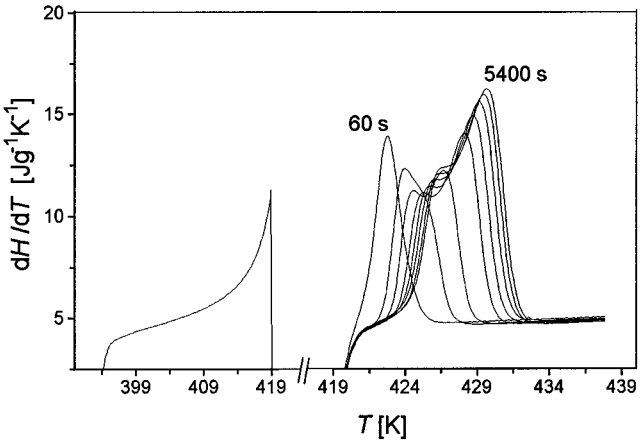

Figure 17. DSC analysis of the recrystallization after melting: Structure evolution as a function of the time of annealing at T = 146 °C as reflected in the DSC curves.

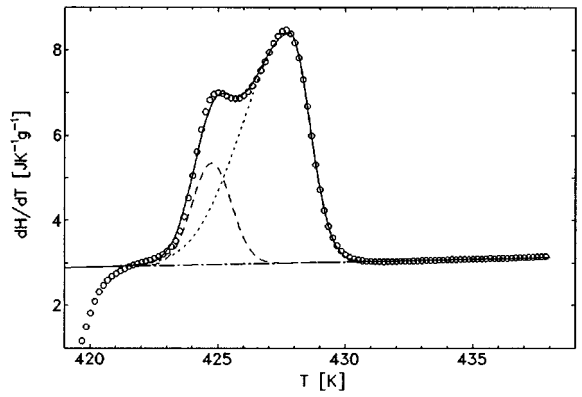

Figure 18. Experiment of Figure 17: Separation of a thermogram into the contributions of the not yet melted and the recrystallized material.

WAXS curves shown in Figure 20. These curves were measured subsequent to a primary crystallization at 120 °C. As indicated by the results shown in the inset, one observes an increase in the intensity of this reflection relative to the others, which is again indicative for a crystal perfectioning during heating.

In order to detect the morphological changes associated with the recrystallization, we carried out corresponding experiments by SAXS. Figure 12 already included indications for a melting−recrystallization process. More detailed results are given in Figure 21.

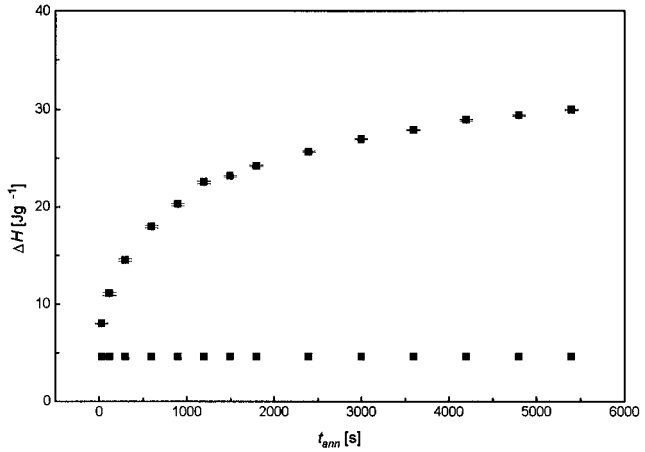

Figure 19. Heat of fusion of the recrystallized material ΔH as a function of the annealing time, derived from the thermograms in Figure 17 (square-tic symbols; the squares at constant level give the contribution of the not yet melted crystallites).

It depicts correlation functions $K(z)$ as measured at the beginning of primary crystallization and then at the end of the melting process, for crystallization temperatures of 122, 128, and 139 °C. For the highest crystallization temperatures we find no change in d_c, as shown by the unchanged width of the base of the self-correlation triangle when comparing the beginning and end. This contrasts with the behavior for T_c = 122 °C, where a clear shift is observed, from the initial 6.5 nm to a final 9 nm. Obviously, the latter value gives the crystal thickness of the recrystallized material. The recrystallized material melts again at 156 °C, as expected for lamellae with this thickness.

Figure 22 shows results for a sample that was only shortly crystallized at 125 °C up to a crystallinity of about 2%. Under these conditions, we observe essentially single crystallites. The curves in the figure show their melting and recrystallization, as reflected in $K(z)$. As for the completely crystallized sample, the first melting occurs around 147 °C. This is followed by a recrystallization of more than half of the original material, which again leads to the formation of crystallites with a thickness of 8.5 nm. These new crystallites then disappear around 156 °C. Hence, we have the same behavior as for the completely crystallized sample.

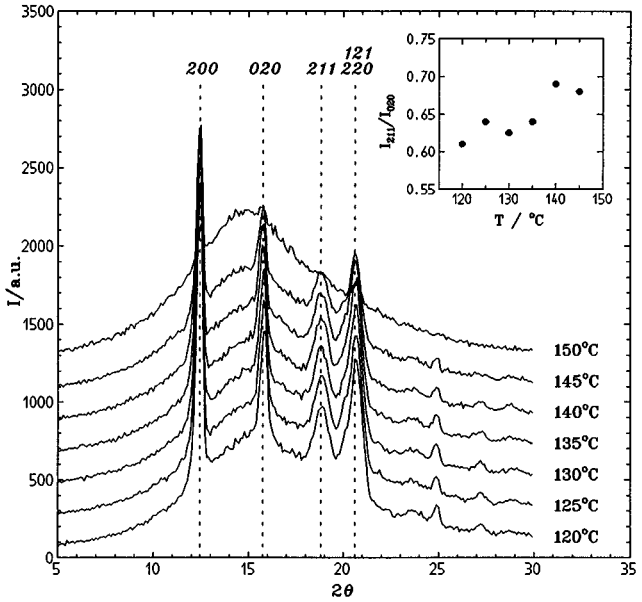

Figure 20. WAXS curves measured on reheating of a sample crystallized at T_c = 120 °C. The insert shows the intensity change of the 211 reflection characteristic for a perfect "type III" crystal. Successive curves are vertically displaced by constant amounts.

3.3. Secondary Crystallization on Cooling. When, after the completion of the primary crystallization, a sample is cooled further, down to room temperature, the crystallization processes continue. This becomes apparent in on-going changes of the small angle X-ray scattering curves. Figure 23 shows these changes as reflected in $K''(z)$. The functions were derived from the SAXS curves measured during a stepwise cooling subsequent to a primary crystallization at 143 °C. After the cooling, samples were heated again to 143 °C. Figure 24 depicts the functions $K''(z)$ obtained during this reheating.

The new feature in these curves is a second peak with a center around 5 nm. It might have already been present at 143 °C as a weak contribution, but then during cooling it greatly increases in weight. At room temperature it reaches a height comparable to the height of the primary peak centered at 8 nm.

The structural changes on cooling are associated with an increase in the specific internal surface O_{ac}. Figure 25 depicts on the left the temperature dependence of the Porod parameter and on the right the temperature dependence of the specific internal surface, obtained by using eqs 9 and 19. The figures include in addition the changes registered during the subsequent reheating. Figure 26 gives the corresponding changes in the crystallinity. These were deduced from the invariant $K(0)$ together with eq 19.

As we find both an increase in the crystallinity as well as in the internal surface, we have clear indication for the insertion mode of secondary crystallization. Cooling leads to the formation of new lamellae that grow between the primary crystallites. Obviously, these secondary crystallites melt again on reheating the sample to the original T_c. We note a splitting between the heating and the cooling curve, indicating that a difference exists between the temperatures of formation and fusion.

A convenient way to learn about the structural changes taking place around a certain temperature is given by calculating the difference between the functions $K''(z)$ obtained during heating and cooling, respectively. By choosing two curves that were measured at the same temperature, one avoids any problems that could arise from the temperature dependent contrast factor $\Delta\rho_e(T)$ included in $K''(z)$. The difference then strictly represents a difference in the distribution function of the distances between interfaces and gives the contribution originating from those crystallites that have not yet formed during cooling but are still stable on heating. Figure 27 presents a set of difference curves derived from the functions $K''(z)$ shown in Figures 23 and 24. At the highest temperatures, 143 and 135 °C, we observe two peaks, the first one located around 10 nm and a second one around 5 nm. The latter stays at a constant position on cooling, whereas the first clearly moves to smaller values. Both seem to merge in the temperature range of 80−90 °C. The first peak apparently continues to move, ending up at about 4 nm at the lowest temperatures. As a comparison with Figure 7 shows, the first peak essentially continues the dependence $d_c(T_c)$ found for the primary crystallites. Its assignment therefore seems to be clear: It gives us the thickness of the secondary crystallites and shows us how it decreases on cooling. On the other hand, the second peak, at 5 nm, appears to be a contribution of amorphous layers, because it is highly improbable that crystallites that are so thin would form at the elevated temperatures. One can identify this value with the minimum thickness of the amorphous layers. Such a minimum thickness certainly exists and it may represent a preferred value. Hence, the general tendencies appear to be clear. Quantitative evaluation does not seem appropriate considering that these data represent something like a third derivative of the correlation function and therefore lack accuracy.

Crystallization processes stop only when the glass transition of the amorphous layers is reached, at around 0 °C. This is demonstrated by the results shown in Figure 28. We have quenched a sample in liquid air after completion of a primary crystallization at 133 °C, and then transferred it into the holder in the Kratky camera preset at 1 °C. SAXS curves were measured twice, after 1.8 h and nearly 3 days time of annealing, and the respective functions $K''(z)$ were determined. In the lower part of Figure 28 we see the difference between the two curves. It shows a peak at 3 nm and a shoulder at 5 nm. We observe also a split minimum, with one contribution at 8 nm and another one around 13 nm. The minimum gives the distribution function of the sum of the thicknesses of a crystallite and an adjacent amorphous layer. It looks appealing to assign the first minimum to the sum of a 3 nm crystallite and the 5 nm amorphous layer and the second to the sum of an 8 nm crystallite together with a newly formed 5 nm amorphous layer. If the 3 nm crystallites grow along the primary 8 nm crystallites at a minimum distance of 5 nm, both contributions would indeed arise.

4. Discussion

The experimental results combined with the broad knowledge in the literature about crystallite structures and morphologies provide us with a sound basis for considerations about the mechanisms effective during the crystallization and melting of this polymer. Indeed, they give a number of clear answers to basic questions and enable us to set up a picture of the controlling processes. We shall develop it step for step in the following.

4.1. Kinetics of Isothermal Crystallization. The kinetics of isothermal crystallization of s-PP agrees with

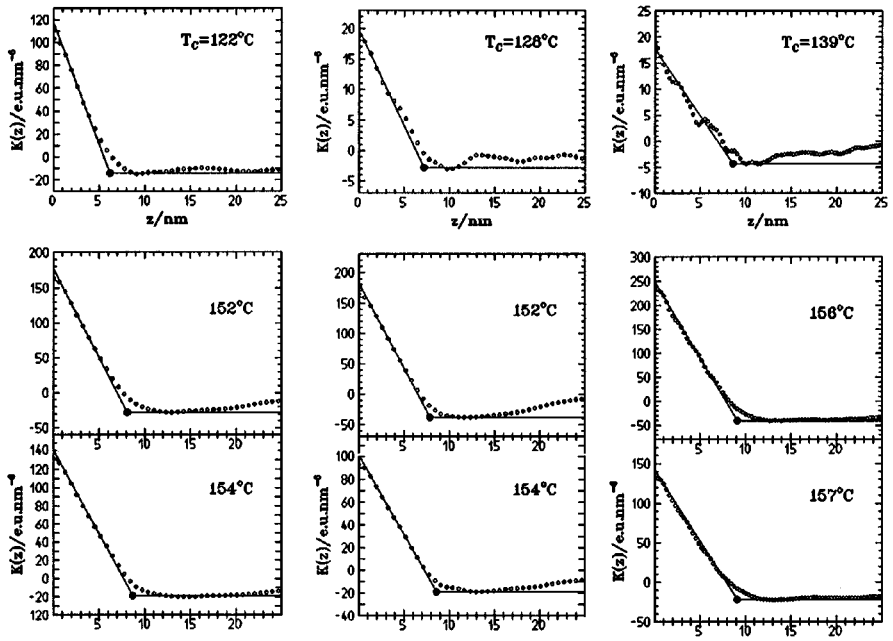

Figure 21. Comparison of the crystallite thicknesses at the beginning of primary crystallization at different T_c's and the end of melting, employing the correlation function $K(z)$.

the behavior commonly found for polymers. Previous work on this substance mainly concerned the temperature range below 120 °C, using DSC. Our experiments go to higher temperatures, and crystallization isotherms are analyzed in terms of the time dependence of the specific internal surface, $O_{ac}(t)$. Characteristic times of crystallization deduced from the Avrami data representation show a temperature dependence that agrees with the data in ref 3 and extends them to higher temperatures. The crystallization behavior is simple in the sense that a change in temperature just results in a shift of the isotherm when we use a logarithmic time axis; i.e., the shape of the curve remains constant and we have only a change in τ. We remark that this simple behavior, although often observed, is not obvious. Overall crystallization kinetics is not controlled by one factor only but includes, in principle, different influences. First, growth takes place in two directions, for s-PP along *a* and *b*, and the two growth faces differ in character. While the *bc*-face looks atomically smooth, the *ac*-face exhibits a curved irregular shape. For an atomically smooth face one may expect layer-by-layer growth, whereas for a rough growth phase face one has to envisage "normal growth" with an attachment of the chain sequences on the always present niches. Furthermore, crystallization starts always with a primary nucleation step. Therefore, how should we interpret the observed simple behavior? The answer is difficult, because observations in the optical microscope give no help. While at lower crystallization temperatures, one observes nucleation and growth of spherulites,[3] no peculiar morphological features are found in the temperature range of our experiments, $T_c \geq 120$ °C. In this situation any geometrical interpretation of the shape of the isotherms as characterized by the Avrami exponent lacks the foundation. We may conclude however, that the ratio of the growth rates along *a* and *b*, which determines the aspect ratio of the crystallites, should remain essentially constant with temperature, as this is a necessary requirement for the similarity property of the growth curves. This implies in the usually given case of an athermal heterogeneous nucleation that the overall crystallization kinetics reflects in their temperature dependence the common change of the two growth rates. It is possible to check this by a comparison with literature data at lower T_c s for samples with a similar molecular weight and content of racemic units.[3] Linear growth rates of the spherulites showing up below 120 °C were measured directly in a microscope. We find for the slope d log τ^{-1}/dT a value close to the reported one.

New knowledge comes from the SAXS curves registered during the isothermal crystallization. The correlation function and the distribution of the distances between the interfaces as reflected in $K''(z)$ tell us quite clearly that the crystal thickness d_c is constant throughout the whole crystallization process, in contrast, for example, to polyethylene where a continuous thickening occurs. In s-PP one can be sure that after completion of the crystallization the sample is homogeneously filled with crystallites of uniform thickness. This thickness increases with increasing crystallization temperature, in the range of our measurements by 50%, from 6 to 9 nm, as shown in Figure 7.

4.2. Melting after Isothermal Crystallization. According to a common view, the generally observed broad melting range of polymers originates from a thickness distribution of the crystallites. Having now a sample with a uniform crystallite thickness or, more accurately speaking, a narrow thickness distribution centered at a sharp maximum, we can check this assumption. Figures 9−11 represent the melting process as monitored by the SAXS experiments during heating. For a sample with a uniform crystallite thickness one would expect a sharp melting point. The observation, however, is clearly different: Melting sets in more or less immediately above the crystallization temperature T_c and then it becomes stronger, up to a maximum that is reached just before the final melting. The curves tell us also that the thickness of the crystallites remains unchanged throughout the heating process. The findings lead to a straightforward conclusion: Obviously, there exist other factors, in addition to the thickness, which affect the stability of the crystallites. Even more important, we learn from the observations that the stability of the crystallites shows great variation. The majority possesses the maximum

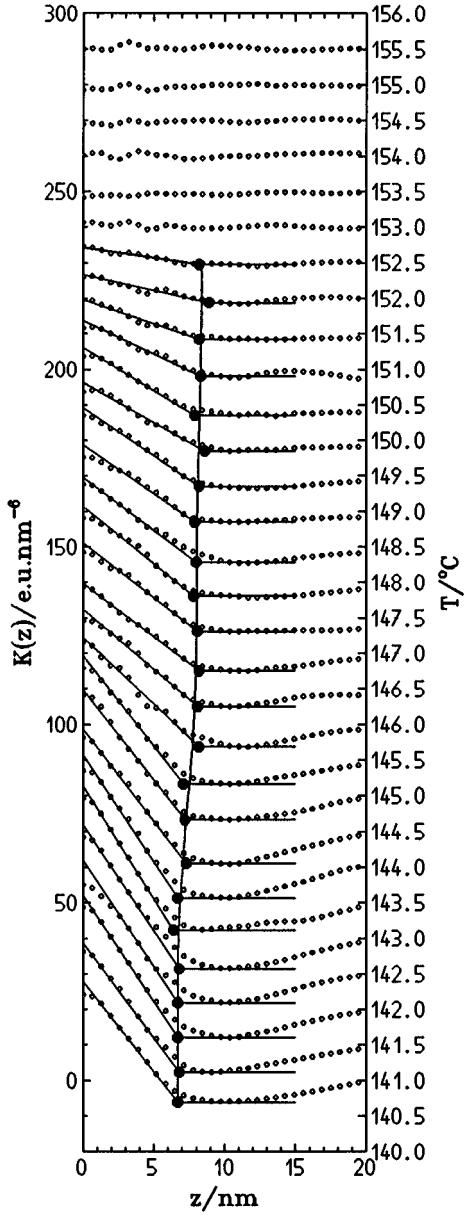

Figure 22. Change of $K(z)$ in the temperature range of recrystallization, observed for a sample shortly crystallized at 125 °C. Successive curves are shifted by constant amounts.

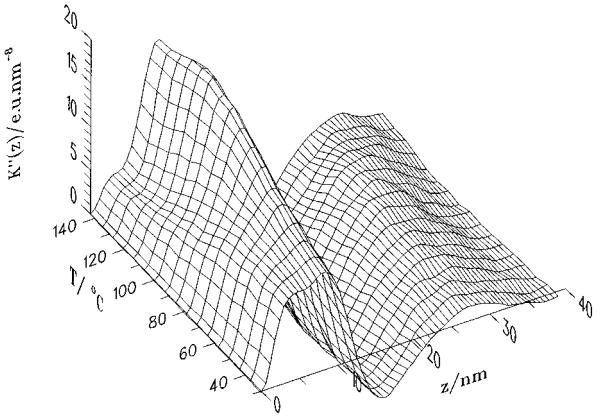

Figure 23. Secondary crystallization during cooling following an isothermal crystallization at 143 °C. Distribution function of interface distances derived from measured SAXS curves.

stability and melts at the high temperature end of the range. However, for others this stability is much reduced so that they can melt already shortly above T_c.

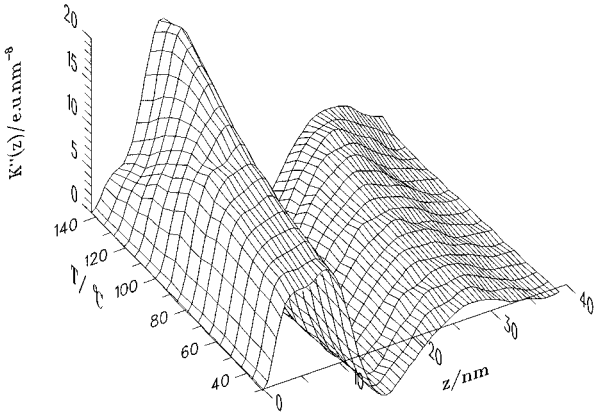

Figure 24. Continuation of the experiment of Figure 23: Structure changes during a reheating back to 143 °C.

The observations are of concern with regard to a central question in the understanding of polymer crystallization, namely that about the cause of the large difference between the temperature of primary crystallization, T_c, and the temperature of the melting peak, T_f. We think that our experiments give an answer. As is known, crystallites of s-PP grow, as polymers in general, with a constant rate, up to the impingement on another crystal. This certainly can only take place under the condition of a constant supercooling; it seems impossible that a distribution of crystallites with temperatures of fusion varying over 20 °C is growing with a uniform velocity. How can these two contradictory observations, the common growth rate of all crystallites and the large variations in the melting points, be reconciled? We see only one answer: Crystallization leads in the first step uniformly to a "native" form of crystals different from the final equilibrium, which is then reached in a second step, by stabilization processes. In the initial form all crystals have equal properties and grow with the same rate. The variations in stability then arise in the next step, if the involved secondary processes are nonuniform. For the structural relaxation, two mechanisms may be envisaged:

(i) In the experiments we have evidence for a perfectioning of the crystal structure. We observed it during heating or annealing at elevated temperatures, but it may also take place directly at the crystallization temperature.

(ii) So far, in the large majority of works, the surface free energy of the crystallites is treated as a constant quantity. In fact, one may well imagine kinetic effects to be present. When the growth face of a crystallite propagates through the melt, the entanglements in front of this face have to be moved away, and they will first become enriched in concentration near to the crystallite surface. Later on, they will become redistributed in the amorphous layer, leading to a relaxation and a gain in mobility in the surface zone. Hence, it looks conveivable to discriminate between a higher kinetic value of the surface free energy and the finally reached lower equilibrium value. One can expect that the difference between the two values increases with the crystallization rate, i.e., with decreasing temperature.

The amount of free energy decrease following from the structural relaxations may vary. As it appears, the majority of the crystallites finally ends up in the equilibrated form but there are others where the relaxation remains incomplete. An interesting insight comes from Figure 9 and a look at the temperature dependence of the ridge related to the long spacing.

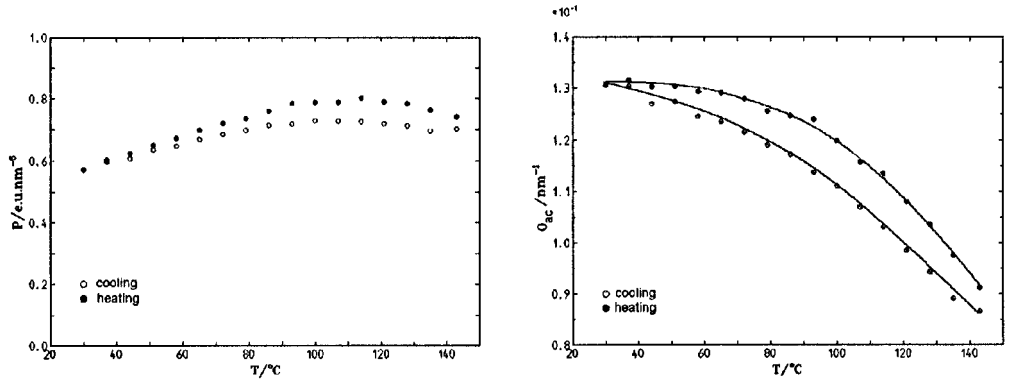

Figure 25. Experiments of Figures 23 and 24: Temperature dependencies of the Porod parameter and the specific internal surface.

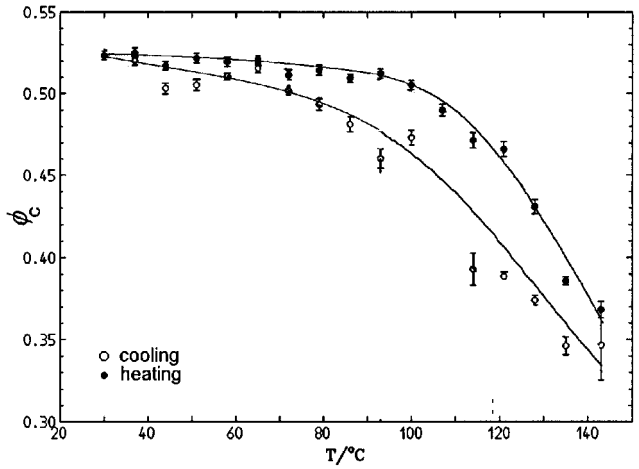

Figure 26. Experiments of Figures 23 and 24: Temperature dependencies of the crystallinity.

While melting proceeds with increasing temperature, the long spacing peak continuously shifts to higher values, and in the range of maximum melting it has already disappeared. Hence, the stability of a crystallite seems to be affected by the distance to the next neighbor. One could think that for small distances, i.e., thin amorphous layers, relaxation may become more difficult and end before the equilibrium state is reached. As a technical remark, if perfectioning processes indeed contribute to the structural relaxation, then SAXS results like Figure 9 may be affected by the related changes in the contrast factor $\Delta\rho_e^2$. The same holds for the time-dependent measurements in Figures 2−5. However, these possible modifications do not influence the determination of d_c so that our main conclusion remains untouched.

The rate of structural relaxation should depend on temperature. In this context it is interesting to have another look at the DSC curves in Figure 16 measured for different heating rates. As was already noted, a decreasing rate leads generally to a sharpening of the first melting peak, indicating that more and more crystals become transformed into the equilibrium state.

The growth rate of the crystallites is determined by the thermodynamic driving force given by the free energy difference between the melt and the growing crystallite, hence, by the supercooling. As already remarked, this supercooling must be constant for all crystallites. Trivially to say, it cannot be larger than the distance between T_c and the temperature where the first crystallites melt again. This happens only a few degrees above T_c, which sets a limit for the supercooling effective during crystal growth.

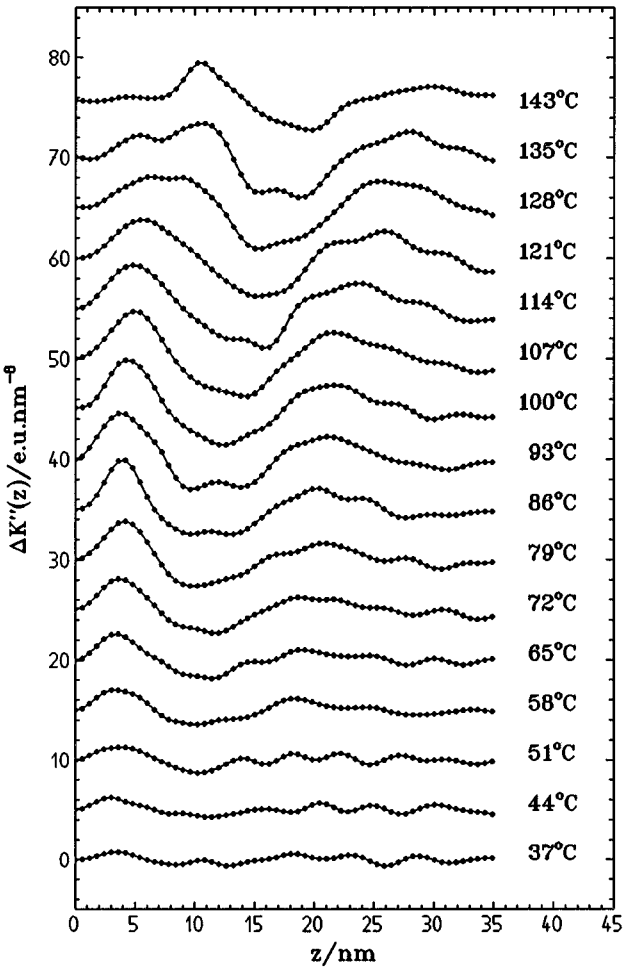

Figure 27. Experiments of Figures 23 and 24: Differences between the functions $K(z)$ obtained during heating and cooling at equal temperatures.

Figure 29 depicts in a common presentation both the dependence of T_c and T_f on the crystallite thickness, in a plot employing the inverse d_c^{-1} as suggested by the Gibbs−Thomson equation. We find two linear dependencies with different slopes. Interestingly, the linear extrapolations of the measured data cross at a finite value of d_c^{-1}. This is a surprising result with consequences, but before discussing it, we consider the melting-recrystallization processes.

4.3. Melting−Recrystallization Process. There is a qualitative difference in kinetics between the primary crystallization starting from an equilibrated melt and the recrystallization subsequent to a crystallite melting: For equal temperatures the latter process

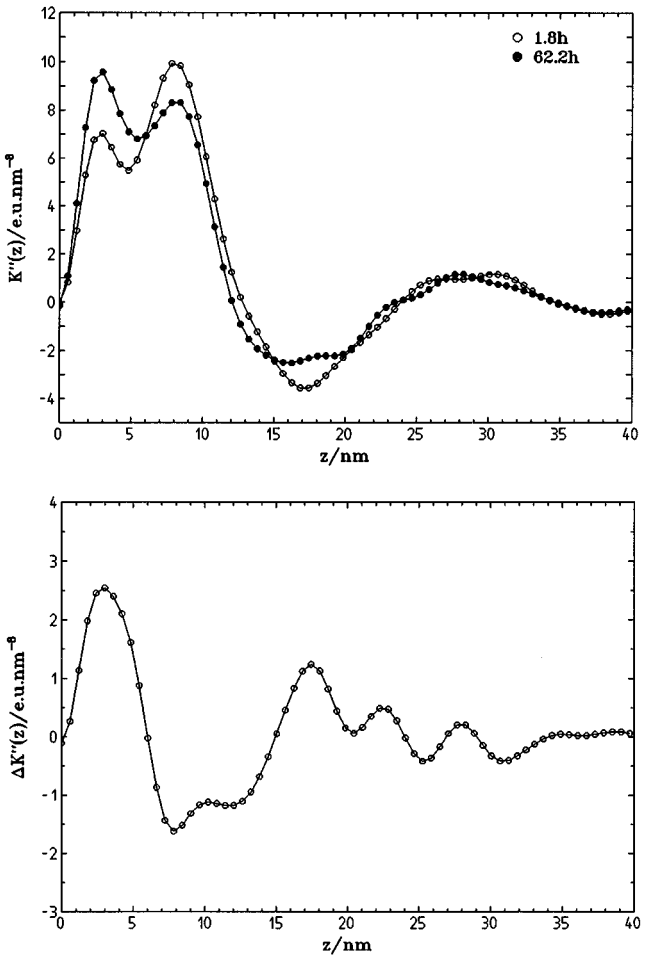

Figure 28. Functions $K(z)$ obtained at 0 °C after 1.8 and 62.2 h of annealing a quenched sample (upper part) and difference function (lower part).

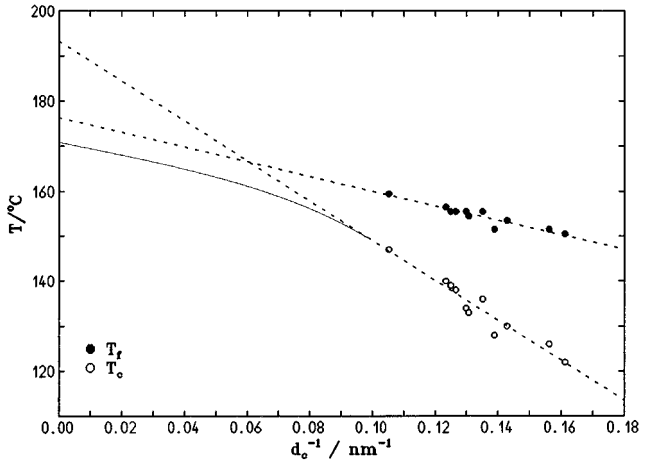

Figure 29. Relations between the inverse crystallite thickness d_c^{-1} and the temperatures of crystalllization T_c and final melting T_f, respectively. The curved line is only schematic and indicates a possible continuation of the dependence $T_c(d_c^{-1})$.

takes place on much shorter time scales. The DSC results of Figure 19 enable us to carry out a quantitative comparison. First we note that for the recrystallization process a nucleation is not necessary, since the largest growth rate is found at the beginning. Here, the crystallinity changes with a rate

$$\frac{\mathrm{d}\phi_c}{\mathrm{d}t} \approx \frac{0.29}{52\ \mathrm{J\ g^{-1}}} \frac{\mathrm{d}\Delta H}{\mathrm{d}t} \approx 2 \times 10^{-4}\ \mathrm{s^{-1}} \qquad (21)$$

On the other hand, for comparison we may estimate the rate of primary crystallization at the same temperature, $T = 146$ °C, using the Avrami equation

$$\phi_c(t) = \phi_c(\infty)\left(1 - \exp\left[-\left(\frac{t}{\tau}\right)^{\beta}\right]\right) \qquad (22)$$

The largest growth rate is found for

$$t/\tau \simeq 1 \qquad (23)$$

and given by

$$\frac{\mathrm{d}\phi_c}{\mathrm{d}t} \simeq \phi_c(\infty)\frac{\beta}{\tau e} \qquad (24)$$

From Figure 6, we find by linear extrapolation

$$\tau = 2.5 \times 10^3\ \mathrm{min} = 1.5 \times 10^5\ \mathrm{s} \qquad (25)$$

and therefore for the maximum rate of change of the crystallinity the result

$$\frac{\mathrm{d}\phi_c}{\mathrm{d}t} \simeq 3 \times 10^{-6}\ \mathrm{s^{-1}} \qquad (26)$$

As we see, there is a large difference, that amounts to at least 2 orders of magnitude.

It is not difficult to give an explanation. As it appears, the structure of the melt immediately after the fusion of a crystallite differs from that of a melt in thermal equilibrium. A basic property of the equilibrated melt is the presence of entanglements. These not only control the viscoelastic properties, but may affect also the transition into a partially crystalline structure. As the entanglements have to be shifted away into the remaining amorphous regions, the progress of the growth front of a crystallite becomes delayed. In reverse, the entangling process, i.e., the process leading to the reestablishment of the entanglement network, requires also a finite time. Therefore, immediately after the melting of a crystallite, the disentangled state is still alive for some time and during this period crystallization rates become much enhanced. If time goes on, the entanglements come back into the region in front of the growth face and, as a consequence, the growth rate progressively decreases. There is a more accurate description of this last point. Generally, the growth rate is determined by the (positive) balance between the rates of attachment and detachment of sequences onto and from the growth face. When the entanglements return, the attachment rate decreases. In order to keep the crystal growing, the detachment rate has to decrease correspondingly and this is achieved by sufficiently increasing the crystal thickness. This exactly is the effect observed in the experiments of Figures 21 and 22.

Regarding the conditions effective during the melting-recrystallization process we recognize what the line $T_f(d_c^{-1})$ in Figure 29 really means: It represents the equilibrium between the equilibrated crystallites and a melt in the disentangled state. This may at first sound like a strange idea, because $T_f(d_c)$ is generally considered as representing the equilibrium melting point of a crystallite with thickness d_c, but we in fact think that this is not strictly true.

Experiments demonstrate, furthermore, that recrystallization proceeds close to this equilibrium line. Compared to the case of primary crystallization we have only a small difference between the temperatures of formation and fusion. The difference shows up directly in the

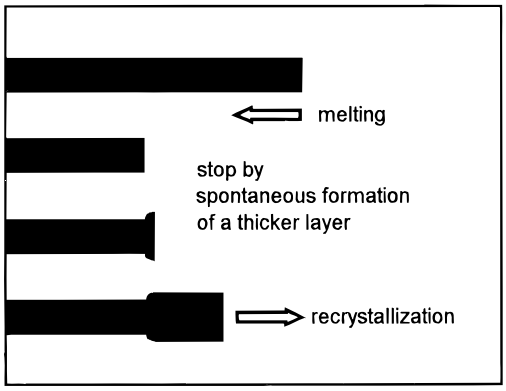

Figure 30. Switching from crystallite melting to growth.

splitting between the first and the second endothermal peak in the DSC curves of Figure 16, which begins with values of about 3 °C. This is far away from the difference anticipated for primary crystallites formed at 146 °C from the equilibrated melt, which, according to Figure 13, would amount to 10 °C.

One may wonder if melting−recrystallization takes place also at lower temperatures during the heating process. Experiments tend to give a negative answer because we did not find during the heating any change in the crystallite thickness. This, however, is not a strict statement because the accuracy could be too low. If melting−recrystallization processes are really absent at lower temperatures, the observed peak sharpening at the low heating rates must be caused by a continuous crystal perfectioning. That the latter process indeed exists is clearly demonstrated by the behavior showing up in Figure 17. The first component found in the curves measured after the annealing at 146 °C representing the not yet melted material is noticeably affected by the time of annealing.

In principle, melting can always turn into crystallization, by the process sketched in Figure 30. Crystallites melt from the surface only, with a rate determined by the superheating $T-T_f$. At some time a thicker layer could form spontaneously on the growth face. If the thickness increase is sufficiently large, recrystallization is initiated and we have a switching from melting to crystallization. For the thicker surface layer, the previous superheating leading to melting turns into a supercooling, now leading to crystallization. In principle this process may always occur during heating. However, its realization requires low enough heating rates.

In summary, dealing with the formation of crystallites in a polymer melt, we encounter two temperatures associated with a given crystal thickness d_c. The first one represents the point of equilibrium between a crystallite in the native, imperfect form and the entangled melt; the second, the temperature of equilibrium between the perfect crystal and a disentangled melt. The crystallization temperature, T_c, is located just below the first; T_f, slightly above the second point.

4.4. Problem of Determining the Equilibrium Melting Point. The data presented in Figure 29 showing a crossing of the lines $T_c(d_c^{-1})$ and $T_f(d_c^{-1})$ at a finite thickness clearly indicate that the Hoffman−Weeks plot is incorrect, at least for s-PP. In this widely used procedure, T_f is plotted against T_c and the point where T_f equals T_c is taken as the equilibrium melting point T_f^∞.[19] We obtain in this way T = 166 °C, in agreement with the literature,[12] but this temperature obviously does not represent T_f^∞. In our picture, this value just gives an estimate of the temperature where the crystal growth rate has become low enough to avoid all kinetic effects, so that perfect crystals are formed immediately.

What can now be done in order to determine the equilibrium melting point of our sample? The answer may be disappointing, as it is, strictly speaking, nothing. Per definition, T_f^∞ represents the temperature where the chemical potentials of a perfect infinitely extended crystal and the relaxed, i.e., entangled, melt are equal to each other. Neither of the two lines $T_f(d_c^{-1})$ and $T_c(d_c^{-1})$ leads in linear extrapolation to this temperature. In one case we have imperfect crystals, in the other an unrelaxed melt. We can only give an upper bound. Since the chemical potential of the equilibrated melt is below that of the nonrelaxed, partially disentangled melt, the equilibrium line is shifted to lower temperatures. The line $T_f(d_c^{-1})$ in Figure 29 is given by

$$T_f = 176\ °C - \frac{163\ °C\ \text{nm}}{d_c} \tag{27}$$

Therefore, we may write $T_f^\infty \leq 176$ °C. In Figure 29 we have also sketched a hypothetical continuation of the dependence $T_c(d_c^{-1})$. The latter function must stay below the line $T_f(d_c^{-1})$, and it ends up exactly at T_f^∞.

Even if we accept 176 °C as a good estimate, i.e., disregard the melt structure effects, we should be reminded that it just represents a value associated with our particular sample. This, although having a high fraction of racemic diads, is still not perfect. Even a small fraction of meso-diads leads to a distinct melting point reduction. According to results obtained by Balbontin et al.[7] this amounts to a shift of about 8 °C per 1% of meso-diads. For our sample, with 3% of meso-diads, we therefore expect an approximate shift of 24 °C against a perfectly syndiotactic polypropylene.

The Gibbs−Thompson equation may still be employed for a determination of the surface free energy of the crystallites in the equilibrated state, if we just consider the slope

$$\frac{dT_f}{dd_c^{-1}} \sim \frac{dT_f}{dn^{-1}} = -\frac{2\sigma_e T_f^\infty}{\Delta h} \tag{28}$$

with Δh the heat of fusion per monomer (C_3H_6), σ_e the free energy reduction per end group, and n the number of monomer units per crystalline stem. The latter follows from

$$n = \frac{d_c}{\Delta z} \tag{29}$$

with

$$\Delta z = 0.185\ \text{nm} \tag{30}$$

giving the height increment per monomer.[4] From the slope of the line in Figure 29 we deduce

$$\left(\frac{2\sigma_e}{\Delta h}\right) = 1.96$$

This value refers to the equilibrium structure of the crystallites. The values associated with the kinetically determined native crystals are obviously much larger,

as indicated by the slope of the line connecting $T_f^\infty = T_c(d_c^{-1} \rightarrow 0)$ and $T_c(d_c^{-1})$. It increases with decreasing temperature, i.e. with increasing growth rate, whereby it is not possible to discriminate between the effects of σ_e and Δh. Probably both give a contribution, in the sense that σ_e increases and Δh decreases.

Just for use in comparisons with other data we give the linear relation between T_c and d_c^{-1} found in our experiments. It reads

$$T_c = 193\ °C - \frac{444\ °C\ nm}{d_c} \tag{31}$$

Introducing the value for Δh given in section 3.1 we may calculate the free energy reduction σ_e due to the end groups. For the equilibrated crystals we obtain

$$\sigma_e = 7.5\ kJ\cdot(mol\ of\ end\ groups)^{-1} = 30.7\ erg\ cm^{-2} \tag{32}$$

(the area per chain is $ab/4 = 0.203\ nm^2$). This value is smaller than the one given by Cheng et al. in ref 6 for lower crystallization temperatures, where the rate of crystallization changes more rapidly.

4.5. Superheating and Times of Crystallite Melting. We already drew attention to the fact that melting of a crystal takes place on its surface only; a melting in the interior does not occur. It is difficult to establish this property in experiments on low molar mass crystals, but clear demonstrations are provided by chain molecular crystals. Here, owing to the extremely low rates of chain attachment and detachment, melting processes can be followed in the microscope in real time, a beautiful example being found in the classical work of Kovacs on fractions of poly(ethylene oxide).[20] As known from the morphological studies, syndiotactic polypropylene forms large single crystals. One may therefore expect that the melting on heating requires a measurable time. Indeed, it shows up in calorimetric measurements as a detectable superheating effect. The DSC curves presented in Figure 16 provide examples. Consider at first the melting curves measured for $T_c = 130$ °C. In the case of the lowest heating rate, the last of the primary crystallites vanishes at 152.5 °C, while for a rate of 10 K/min, that is still low enough to eliminate heat conduction effects within the apparatus, they persist up to 155.5 °C. This indicates a superheating of 3 °C. For the given heating rate it corresponds to a time required for melting of 18 s.

There is a second route to determine the superheating during the crystallite melting, and it uses MDSC measurements. A full discussion of the information content of MDSC curves like those shown in Figure 15 will be provided elsewhere, in a separate paper, and we sketch here only briefly the basis of the evaluation. Consider the heat flux during melting of a crystallite. Under isothermal conditions it is solely due to the melting process. Melting takes place on the lateral faces of the crystallites and we may write

$$\left(\frac{dQ}{dt}\right)_0 = \frac{\Delta h}{v_m} O_{lf} u_- \tag{33}$$

Here, O_{lf} describes the total area of lateral crystal faces contributing to the melting process. The melting leads to a shift of the lateral faces into the crystal interior and we describe the displacement per second by the parameter u_-. Further parameters in the equation are the heat of melting per monomer, Δh, and the monomer volume, v_m. The origin of this equation is obvious and it should be generally valid.

Next consider the additional effect of a superimposed temperature modulation with frequency ω and amplitude ΔT_0. It leads to a fluctuation of the heat flowing into the sample described by

$$\left(\frac{dQ}{dt}\right)_\omega \sin \omega t = \frac{\Delta h}{v_m} \Delta T_0 O_{lf} \frac{du_-}{dT} \sin \omega t \tag{34}$$

The ratio between the mean value of the heat flow and the amplitude of the fluctuating component follows as

$$\frac{\left(\frac{dQ}{dt}\right)_\omega}{\left(\frac{dQ}{dt}\right)_0} = \frac{\Delta T_0 \frac{du_-}{dT}}{u_-} \tag{35}$$

If rather than using isothermal conditions, the sample is slowly heated under superposition of temperature modulations as described by the program eq 1, melting takes place at temperatures above the equilibrium melting point. For small superheatings we may assume a linear relation between the rate of melting and the superheating

$$u_- = \frac{du_-}{dT}(T - T_f) \tag{36}$$

This leads to

$$\frac{\left(\frac{dQ}{dt}\right)_\omega}{\left(\frac{dQ}{dt}\right)_0} = \frac{\Delta T_0}{T - T_f} \tag{37}$$

whereby (dQ/dt) is understood as representing only the heat flow due to melting.

In the experiment of Figure 15 the results are given in terms of the mean heat capacity c_l and the dynamic heat capacities c_v' and c_v''. The fluctuating part of the heat flow during a crystallite melting relates to the imaginary part of the dynamic heat capacity, being given by

$$c_v'' = \frac{\left(\frac{dQ}{dt}\right)_\omega}{\Delta T_0 \omega} \tag{38}$$

For the part of the mean heat capacity associated with the melting we have

$$c_l = \frac{\left(\frac{dQ}{dt}\right)}{\beta} \tag{39}$$

We therefore obtain for the ratio between these two quantities

$$\frac{c_v''}{c_l} = \frac{\beta}{\omega(T - T_f)} \tag{40}$$

If a sample is heated and crystallites start to melt, the superheating varies in time. For each crystal, melting sets in at the equilibrium melting point; then the superheating increases linearly to a certain maximum that depends on the parameter du_-/dT, the heating rate β, and the crystal size. The calorimeter measures an

average. Hence, we write

$$\frac{c_v''}{c_1} = \frac{\beta}{\omega\overline{(T - T_f)}} \tag{41}$$

The average superheating and the average time required for the crystallite melting are related by

$$\overline{(T - T_f)} = \beta\Delta t_f/2 \tag{42}$$

Therefore, we can also write

$$\frac{c_v''}{c_1} = \frac{2}{\omega\Delta t_f} \tag{43}$$

Hence, MDSC experiments provide us with a means to determine superheating effects and melting times of crystallites in a sample. For low molar mass crystals both quantities can be immeasurably short. Not so for polymers, where melting requires a finite time.

Let us now have a look at of Figure 15. We find in the range of the melting peak for the ratio of the heat capacities a value

$$\frac{c_v''}{c_l} = 0.22$$

This was obtained for a heating rate $\beta = 0.5$ K min^{-1} and a frequency of the modulation $\omega = 2\pi/96$s. Hence, the average superheating is

$$\overline{(T - T_f)} = 0.6 \text{ K}$$

implying that the average time required for a crystallite melting is $\overline{\Delta t_f} = 72$ s. This is indeed a remarkably long time.

We can compare this result with the direct observation cited above. The latter refers to another heating rate, 10 K/min rather than 0.5 K/min. It is possible to estimate the related change. For a crystal of length l the time required for melting is given by

$$l = \beta\frac{du_-}{dT}\frac{\Delta t_f^2}{2} \tag{44}$$

Accordingly, Δt_f changes with the heating rate as

$$\Delta t_f \sim \beta^{-1/2} \tag{45}$$

Consequently, the superheating changes with the heating rate as

$$\overline{(T - T_f)} = \beta\Delta t_f/2 \sim \beta^{1/2} \tag{46}$$

Using this relation we arrive at

$$\overline{(T - T_f)} = 2.8 \text{ K}$$

in perfect agreement with the direct observation.

Interestingly, the superheating effect becomes diminished when decreasing the crystallization temperature. For a heating rate of 10 K min^{-1} we observe at $T_c =$ 120 °C a superheating $\Delta T \approx 1$ °C and at $T_c = 125$ °C a $\Delta T \approx 2$ °C. This would correspond to times of melting $\Delta t_f \approx 6$ s and $\Delta t_f \approx 12$ s for these two temperatures. This decrease in the melting time makes sense. Just remind that decreasing crystallization temperatures lead to smaller thicknesses and higher crystallization rates. In correspondence to that we may anticipate also a higher melting rate.

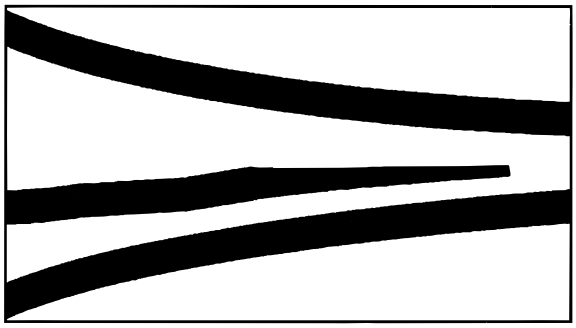

Figure 31. Mechanism of crystal growth during secondary crystallization.

It appears that the average superheating is not constant during the heating. For temperatures below 146 °C, i.e., outside the region of the melting peak, we find a ratio

$$\frac{c_v''}{c_l} \approx 1$$

corresponding to an average superheating

$$\overline{(T - T_f)} = 0.13 \text{ K}$$

and an average melting time $\Delta t_f = 16$ s. One may understand this result as indicating that the less stable crystals have a smaller size.

The observed values for the superheating have an important implication. As we have employed a modulation amplitude of 0.2 K, which is in the same order or larger than $\overline{(T - T_f)}$, during many of the cycles the melting point is crossed. The existence of a dynamic signal under these conditions is clearly indicative for a continuous transition from melting to crystallization at the growth face when switching from superheating to supercooling. "Normal growth" on rough growth faces behaves like that, "layer growth" controlled by secondary nucleation would not have this property.

4.6. Insertion Mode Crystallization. According to the experiment of Figures 23−26 we had at the end of the isothermal crystallization at 143 °C, before starting the cooling process, stacks of crystallites with a thickness $d_c = 8$ nm, setting up a two-phase structure with a crystallinity $\phi_c = 0.34$ and a specific internal surface $O_{ac} = 8.6 \times 10^{-2}$ nm^{-1}. The amorphous regions show a broad thickness distribution with an average of 15.5 nm. The secondary crystallization during cooling to room temperature then results in an increase in the specific internal surface of $\Delta O_{ac} = 0.045$ nm^{-1} and in the crystallinity of $\Delta\phi_c = 0.17$. The changes are brought about by introducing additional crystallites, with thicknesses starting at values around 10 nm, that is similar to the primary crystallites, and then decreasing steadily, down to 4 nm at room temperature. Probably many of the new crystallites develop just by continuation of already existing ones.

We have also evidence for the occurrence of a minimum thickness of the amorphous regions with a value around 5 nm. This seems to be a preferred distance in the broad distribution, therefore showing up as a peak in $K''(z)$. Its weight increases on cooling, indicating that more and more crystallites realize a distance according

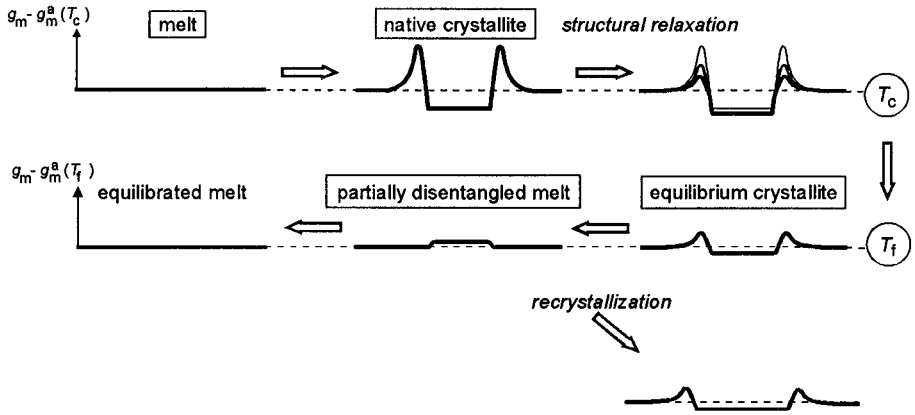

Figure 32. Four-state scheme for treating polymer crystallization and melting, indicating the processes taking place at the temperatures of crystallization and the melting peak, T_c and T_f.

to this minimum value. Figure 31 summarizes all these observations in a simple sketch.

Two points are to be especially noted. First, as already remarked, we find that the dependence of the crystallite thickness on temperature during secondary crystallization essentially continues the former dependence found for the primary crystallization. Equation 31, which describes the primary crystallization, predicts for 100 °C a value of 5 nm and for 0 °C a value of 2.3 nm. The values determined during secondary crystallization are close to these predictions. As another observation, one may recognize that the secondary crystallites do not reach the stability of the primary crystallites because, as is to be noted, the difference $T_f - T_c$ is definitely smaller. For example, secondary crystallites grown at 120 °C are completely molten already at 135 °C compared to 149 °C found for a primary crystallite grown at the same temperature. In our view, structure relaxation is hindered if two crystallites closely approach each other, down to the minimum distance. In the thinnest amorphous layers the entanglement density is at a maximum and a redistribution down to the values in the relaxed melt is no longer possible. One may also generally consider the increasing entanglement density produced when two primary crystallites approach each other as a main controlling factor. Already during primary crystallization, a lamella growing in between two already existing ones can grow only to the limit where a critical density of the entanglements is reached. Secondary crystallization then just means a continuation under the action of the increased thermodynamic driving force provided at the lower temperatures.

5. Conclusions

We understand our experiments as teaching us that crystallization in syndiotactic polypropylene, in the form of the primary and secondary crystallization or the recrystallization after melting, always takes place with a normal, i.e., small undercooling. The peculiarities in behavior arise from the fact that the phases involved in the primary crystallization and the final melting are not the same ones. Primary crystallites grow near to the equilibrium between the entangled equilibrated melt and an imperfect "native crystallite". In contrast to this, the main part of the melting occurs near the equilibrium between the crystallite in its equilibrium state and a melt that is still disentangled in the decisive region in front of the growth face. The large difference between the temperature of formation of the primary crystallites, T_c, and the temperature of final melting, T_f, originates under these conditions from the structural relaxation of the crystallites both at their surfaces and in the interior, and additionally, from the upward shift of the chemical potential of the melt following from the disentangling enforced by the crystallization process. Hence, in order to properly deal with the summary of all observations we need a four-state scheme with two states for the melt, given by the entangled equilibrium state and the disentangled temporary state, and two states for the crystallites, the native state at the time of formation and the equilibrated state reached for the majority of crystallites at the end of the structural relaxation processes. Figure 32 gives a sketch of the proposed scenario, with all the different phases and processes. Curves depict the course of the local Gibbs free energy through a crystallite, showing a minimum in the interior and maxima in the surface regions.

Taken as a whole the scheme might be new, but of course, it is composed of processes that have been known and discussed for a very long time. We can only cite a few works, selected more or less by chance. To begin with, the idea of an initial formation of imperfect crystals immediately followed by a perfectioning is expressed in Wunderlich's book[21] (Chapter 6.1.6) and supported by several observations. These processes show up, for example, when employing fast calorimetry on polyethylene (Figure VI.24) or, even more directly, in the existence of a perturbed boundary zone in growing crystals of poly(ethylene oxide) (work of Kovacs, Figure VI.27). An effect of the surface structure on the stability of polymer crystallites was deduced by Holdsworth and Turner-Jones[22] from X-ray studies on poly(ethylene terephthalate). The melting−recrystallization process has found much interest already in the sixties, in particular in works of Stuart and Zachmann.[23] Skepticism against the Hoffman−Weeks procedure has also existed for a long time, and is well substantiated in Wunderlich's book. In fact, the tentative continuation of the curve $T_c(d_c^{-1})$ in Figure 29 is not pure speculation, but supported by observations on several polymers (it-polystyrene, poly(vinylidene fluoride), poly(butadiene)), all of them collected in ref 21 (Chapter 9.3.2). Finally, direct evidence for the occurrence of states intermediate between the equilibrated melt and ordered crystallites both during crystallization and melting is provided in a work of Kanig[24] on polyethylene. Employing a rapid staining technique in a time-dependent electron microscopic investigation, he could observe such intermediate states and addressed them as "smectic".

We do not think that it would be appropriate to analyze the kinetic data using the Hoffman−Lauritzen

treatment. The basis for its application is lacking, in many respects:

•The growth face is rough, which leads to normal growth rather than layer-by-layer growth.

•Growth control by secondary nucleation produces an asymmetry between melting and crystallization by necessitating a finite supercooling before the onset of growth. This is contradicted by both the immediate onset of recrystallization after melting, and the existence of a dynamic DSC signal indicative of a smooth transition between melting and crystallization.

•A main factor in the crystallization kinetics is the dependence of the crystallite thickness on T_c. We find clear deviations from the usually assumed proportionality between d_c and the inverse supercooling, originating from a continuous change of the properties of the initial crystallites.

In an attempt to deal with the observations and to evaluate the kinetic data we developed another theoretical concept. It is presented in a separate paper.[25]

One may wonder if the conclusions are restricted to s-PP. We do not think so, considering that the overall behavior is absolutely in line with the usual observations on polymer systems. It is only that in other polymers further complications may arise, as for example, in polyethylene the solid state thickening processes. The four-state scheme suggested by our studies on s-PP could thus well have a wider significance.

Acknowledgment. Support of this work by the Deutsche Forschungsgemeinschaft (Graduiertenkolleg "Strukturbildung in Makromolekularen Systemen" and SFB 60) is gratefully acknowledged. Thanks are also due to the "Fonds der Chemischen Industrie" for financial help.

References and Notes

(1) Ewen, J. A.; Jones, R. L.; Razavi, A.; Ferrara, J. D. *J. Am. Chem. Soc.* **1988**, *110*, 6255.

(2) Lovinger, A. J.; Lotz, B.; Davis, D. D.; Schumacher, M. *Macromolecules* **1994**, *27*, *6603*.

(3) Rodriguez-Arnold, J.; Bu, Z.; Chen, S. Z. D.; Hsieh, E. T.; Johnson, T. W. Geerts, R. G.; Palackal, S. J.; Hawley, G. R.; Welch, M. B. *Polymer*, **1994**, *35*, 5194.

(4) Corradini, P.; Natta, G.; Ganis, P. Temussi, P. A. *J. Polym. Sci., Part C* **1967**, *16*, 2477.

(5) Lotz, B.; Wittmann, J. C.; Lovinger, A. J. *Polymer* **1996**, *37*, 4979.

(6) Bu, Z.; Yoon, Y.; Ho, R.-M.; Zhou, W.; Jangchud, I.; Eby, R. K.; Cheng, S. Z. D.; Hsieh, E. T.; Johnson, T. W.; Geerts, R. G.; Palackal, S. J.; Hawley, G. R.; Welch, M. B. *Macromolecules* **1996**, *29*, 6575.

(7) Balbontin, G.; Dainelli, D.; Galimbert, M.; Paganetto, G. *Makromol. Chem.* **1992**, *193*, 693.

(8) Haftka, S. Konnecke, K. *J. Macromol. Sci., Phys. B* **1991**, *30*, 319.

(9) Albrecht, T.; Strobl, G. R. *Macromolecules* **1995**, *28*, 5827.

(10) Albrecht, T.; Strobl, G. R. *Macromolecules* **1996**, *29*, 783.

(11) Sakata, Y.; Unwin, A. P.; Ward, I. M. *J. Mater. Sci.* **1995**, *30*, 5841.

(12) Marigo, A.; Marega, C.; Zannetti, R. *Macromol. Chem. Rapid Commun.* **1994**, *15*, 225.

(13) Strobl, G. *The Physics of Polymers*; Springer: Berlin, 1996.

(14) Thomann, R.; Wang, C.; Kressler, J.; Jüngling, S.; Mülhaupt, R. *Polymer* **1995**, *36*, 3795.

(15) Strobl, G. *Acta Crystallogr.* **1970**, *A26*, 367.

(16) Reading, M. *Trends Polym. Sci.* **1993**, *1*, 248.

(17) Ruland, W. *Colloid Polym. Sci.* **1977**, *255*, 417.

(18) Lovinger, A. J.; Lotz, B.; Davis, D. D.; Padden, F. J., Jr. *Macromolecules* **1993**, *26*, 3494.

(19) Hoffman, J. D.; Weeks, J. J. *J. Res. Natl. Bur. Stand., Sect. A* **1962**, *66*, 13.

(20) Kovacs, A. J.; Straupe, C.; Gonthier, A. *J. Polym. Sci., Polym. Symp.* **1977**, *59*, 31.

(21) Wunderlich, B. *Macrmolecules Physics*; Academic Press: New York, 1976; Vol. 2, Chapter 5.3.

(22) Holdsworth, P.; Turner-Jones, A. *Polymer* **1971**, *12*, 195.

(23) Zachmann, G.; Stuart, H. A. *Makromol. Chem.* **1960**, *8*, 131.

(24) Kanig, G. *Colloid Polym. Sci.* **1991**, *269*, 1118.

(25) Strobl, G. Acta Polym., in press.

MA9703923